PHYSICAL REVIEW B

CONDENSED MATTER

THIRD SERIES, VOLUME 39, NUMBER 8 15 MARCH 1989-I

Electronic-structure calculation for metals by local optimization

C. Woodward,* B. I. Min,† R. Benedek, and J. Garner‡

Materials Science Division, Argonne National Laboratory, Argonne, Illinois 60439-4843

(Received 29 September 1988)

Recent work by Car and Parrinello has generated considerable interest in the calculation of electronic structure by nonlinear optimization. The technique introduced by these authors, dynamical simulated annealing, is designed for problems that involve energy barriers. When local optimization suffices to determine the energy minimum, more direct methods are available. In this paper we apply the algorithm suggested by Williams and Soler to calculate the electronic structure of metals, using a plane-wave expansion for the electronic orbitals and an electron-ion pseudopotential of the Kleinman-Bylander form. Radial pseudopotentials were taken from the compilation of Bachelet, Hamann, and Schlüter. Calculations are performed to optimize the electronic structure (i) with fixed atomic configuration, or (ii) with the atomic volume being optimized simultaneously. It is found that the dual optimization (ii) converges in essentially the same number of steps as the static lattice optimization (i). Numerical results are presented for Li, K, Al, and simple-cubic P.

I. INTRODUCTION

Most techniques for the calculation of electronic structure in solids involve matrix diagonalization. Since the numerical effort in diagonalization scales as the cube of the matrix size, these techniques can become inefficient for systems with large unit cells or low symmetry. Alternative strategies have been designed to minimize or avoid the diagonalization bottleneck, including the following.

(i) Construct an optimized basis of minimal size. The linear muffin-tin orbitals (LMTO) tight-binding formalism[1] represents one such scheme; see Refs. 2 and 3.

(ii) Apply iterative algorithms constructed to yield only the lowest-lying eigenstates.[4] Few applications to solids have been made to date.

(iii) Determine the eigenstates by nonlinear optimization, as in the widely noted work of Car and Parrinello,[5,6] or in extensions thereto.[7,8]

We develop in this paper a procedure for calculating electronic structure in metals by optimization, with the objective of treating systems with large unit cells. An attractive feature of the method is the capability of simultaneous optimization of the electronic structure and the atomic configuration. We demonstrate this feature by optimizing both the lattice constant and the electronic states in parallel. Our procedure is also expected to be compatible with molecular dynamics simulation, but that application is not explored in this paper.

Electronic states are calculated by the equation-of-motion method proposed by Williams and Soler (WS),[7] which we have found superior to several other possible optimization methods.[9] Electronic wave functions are expanded in plane waves[10] in order to exploit the efficiency of fast Fourier transformation.[5] A norm-conserving pseudopotential cast in the Bylander-Kleinman form[11,12] is used to represent the electron-ion interaction. Brillouin-zone integrations are performed by a Gaussian-broadening method.[2,13] As presently formulated, our techniques are restricted to *s-p*-bonded systems; however, they could be extended to *d*- and possibly *f*-electron materials with a mixed-basis representation.[14]

The equations of motion employed in our electronic-structure optimizations are presented in Sec. II. In Sec. II A we discuss the WS algorithm. Most previous applications of optimization methods[5,6,12,15] have dealt with semiconductors; Sec. II B outlines the adaptation of the present approach to treat open-shell systems. A brief discussion of pseudopotentials is given in Sec. II C. Tests and applications to pure metals are presented in Sec. III, and a discussion of the results is given in Sec. IV. Appendix A describes the formulation of the Gaussian-broadening method and Appendix B outlines the calculation of total energy and pressure.

II. OPTIMIZATION METHODS

A. Williams-Soler algorithm

Car and Parrinello[5] showed that "simulated annealing," originally applied in the context of Monte Carlo algorithms, could also be adapted to deterministic dynamical models. Their main objective was to develop an *ab in-*

itio formulation of molecular dynamics, in which the electronic contributions to the atomic forces are determined within the local-density approximation. They demonstrated that the Lagrangian equations of motion for the ions, in conjunction with the (pseudo)Lagrangian equations of motion

$$\partial^2\Psi_i/\partial t^2 = -H\Psi_i + \sum_j \Lambda_{ij}\Psi_j \ , \tag{1}$$

for the electrons, describe the dynamics of classical ions moving in a background of adiabatic electrons. In Eq. (1), H is the one-electron (Kohn-Sham) Hamiltonian, Ψ_i are the occupied orbitals, and Λ_{ij} are Lagrange multipliers that ensure orthonormality (the fictitious masses are set to unity here).

Another application of simulated annealing, more directly relevant to our present purpose, is the calculation of electronic orbitals by integrating Eq. (1) and quenching the "fictitious" kinetic energy at appropriate intervals.[5] Payne *et al.*[8] developed an algorithm for analytically integrating Eq. (1), which substantially improved the efficiency of this procedure. Williams and Soler[7] recognized that the Payne *et al.* algorithm, in effect, performs a local optimization, and proposed a more direct form of fictitious dynamics, which eliminates the need to quench,

$$\partial\Psi_i/\partial t = -H\Psi_i + \sum_j \Lambda_{ij}\Psi_j \ . \tag{2}$$

Equation (2), which can be derived from a steepest-descents condition,[6,7] is simply the imaginary-time Schrödinger equation, for which excited-state solutions decay exponentially.[16] Employing the orthonormality constraint $\Lambda_{ij}=H_{ji}$, we can rewrite Eq. (2) in the form

$$\partial\Psi_i/\partial t = -(1-P_N)H\Psi_i \ , \tag{3}$$

where

$$P_N \equiv \sum_{i=1}^{N} |\Psi_i\rangle\langle\Psi_i|$$

projects onto the Hilbert subspace of the N occupied states $\Psi_i(t)$. With the help of Eq. (3), the time derivative of the energy can be written

$$dE/dt = -2\sum_{i=1}^{N} \langle i|H(1-P_N)H|i\rangle \ . \tag{4}$$

Since $(1-P_N)\geq 0$, it follows that $dE/dt \leq 0$, and thus the solution to Eq. (2) monotonically approaches an energy minimum.[17]

It is convenient to expand the electron orbitals in terms of plane waves,

$$\Psi_i(\mathbf{r},t) = \sum \Psi_i(\mathbf{G},t)\exp(i[\mathbf{k}+\mathbf{G}]\cdot\mathbf{r}) \ . \tag{5}$$

Here, the subscript i denotes both the band index ν and the wave vector $\mathbf{k}$. Substituting Eq. (5) into the EOM, Eq. (2), we obtain

$$\partial\Psi_i(\mathbf{G},t)/\partial t = -(H_{\mathbf{GG}}-\Lambda_{ii})\Psi_i(\mathbf{G},t)+\beta_i(\mathbf{G},t) \ , \tag{6}$$

where

$$\beta_i(\mathbf{G},t) = -\sum_{\mathbf{G}'}{}' H_{\mathbf{GG}'}\Psi_i(\mathbf{G}',t) + \sum_j{}' \Lambda_{ij}\Psi_j(\mathbf{G},t) \ . \tag{7}$$

The primes on the summations in Eq. (7) indicate that the diagonal terms $H_{\mathbf{GG}}$ and Λ_{ii} are omitted.[18] If the parameters $H_{\mathbf{GG}}$, Λ_{ii}, and $\beta_i(\mathbf{G},t)$ are treated as constants,[7,19] Eq. (6) can be integrated analytically,

$$\Psi_i(\mathbf{G},t+h)+\Psi_i(\mathbf{G},t)+F_i(\mathbf{G},t)f(\mathbf{G},t,h)h \ , \tag{8a}$$

where the residual vector F is defined as

$$F_i(\mathbf{G},t) = -\sum_{\mathbf{G}',j}{}' (H_{\mathbf{GG}'}\delta_{ij}-\Lambda_{ij}\delta_{\mathbf{GG}'})\Psi_j(\mathbf{G}',t) \ , \tag{8b}$$

and $f(\mathbf{G},t,h)\equiv f(x)\equiv(e^x-1)/x$, with $x=-(H_{\mathbf{GG}}-\Lambda_{ii})h$. Equation (8) is utilized as follows. After the selection of initial states $\Psi_i(\mathbf{G}, t=0)$, Eq. (8) is applied iteratively until convergence is achieved; following each iteration, the states are orthonormalized by the Gram-Schmidt method and a new set of potentials, Hamiltonian matrix elements, and Lagrange multipliers are determined. It was noted recently[20] that Gram-Schmidt orthogonalization removes any spurious symmetry inadvertently "built in" to the initial states.

Equation (8) was written by Williams and Soler[7] in a slightly different form. The present form shows clearly the relationship of the approach to the "method of steepest descents."[21] The condition of vanishing residuals, $F_i(\mathbf{G})=0$, is simply a restatement of the Kohn-Sham eigenvalue equation (for states related to Kohn-Sham orbitals by a unitary transformation.) Further, we observe that if f is set equal to unity, Eq. (8) reduces to the method of steepest descents,[21] i.e., the "displacement" in a given iteration is parallel to the residual F. Equation (8) in conjunction with the definition $f(x)\equiv(e^x-1)/x$ improves on the steepest-descents method by including the curvature of the steepest-descents path. Since the time dependence of $H_{\mathbf{GG}}$, Λ_{ii}, and $\beta_i(\mathbf{G},t)$ are neglected, however, this integration is only approximate and a maximum "time interval" h exists for which the method remains stable, i.e., for which the total energy $E(t+h)<E(t)$. Nevertheless, values of h exist for which Eq. (8) is stable and converges much faster, typically by a factor of 5 or 10, than the method of steepest descents.[10,21,22]

Alternative methods of solution to Eq. (7) are available. For example, the Born-Dyson perturbation series can be applied, treating $(\partial/\partial t - H_{\mathbf{GG}}+\Lambda_{ii})^{-1}$ as the Green's function and $\beta_i(\mathbf{G},t)$ as the perturbation.[23] Unlike Eq. (8), however, finite-order Born series expansions converge only approximately to the Kohn-Sham orbitals as $t\rightarrow\infty$. A more detailed discussion of the relative performance of different methods of solution to Eq. (2) will be presented elsewhere.[9]

B. Adaptation to metals

As mentioned above, most existing optimization calculations[5,6,12,15] have been on semiconductors. Calculations for metals entail additional complications because of the Fermi surface and the tendency of self-consistency algorithms to exhibit instabilities. We have adopted the fol-

lowing procedures in order to treat metals. First, the Gaussian-broadening method[2,13] is applied to zone integrations. Although tetrahedron integration methods are preferred in conventional electronic structure calculations, they require a larger number of k points to converge.[24] The electronic charge density is expressed in the form

$$n(\mathbf{r})=\sum_{\nu,\mathbf{k}}|\phi_{\nu,\mathbf{k}}(\mathbf{r})|^2 w(\nu,\mathbf{k}) , \tag{9}$$

where $\epsilon_{\nu,\mathbf{k}}$ is the eigenvalue corresponding to the Kohn-Sham orbital $\phi_{\nu,\mathbf{k}}$. The summation is over the band index ν and over n_k points in the Brillouin zone.[25] The weight $w(\nu,\mathbf{k})$ is the product of a volume factor $\Omega(\mathbf{k})$ and an occupancy factor $z(\epsilon_F-\epsilon_{\nu,\mathbf{k}})$; $w(\nu,\mathbf{k})$ thus also depends implicitly on the Fermi level ϵ_F. For accurate sampling, values of $n_k \geq 5$ are employed so as to include at least one low symmetry point. An explicit relation for the occupancy factor z is derived in Appendix A. For each k point, Eq. (9) is summed over a sufficient number of bands $n_\nu(\mathbf{k})$ to include the low-lying excited states, which have a finite occupancy factor z in the Gaussian-broadening scheme.

The (converged) orbitals $\Psi_{\nu,\mathbf{k}}$ calculated by the methods of the previous section will generally differ from the eigenfunctions of H by a unitary transformation. To obtain the Kohn-Sham orbitals $\phi_{\nu,\mathbf{k}}$ that enter Eq. (9), a diagonalization of the Hamiltonian matrix H_{ij} $(=\Lambda_{ji})$ is performed in the $[n_\nu(\mathbf{k})$-dimensional] subspace of the orbitals $\Psi_{\nu,\mathbf{k}}$. Thus, after each iteration of Eq. (8), a new charge density $n(\mathbf{r})$ is calculated with the (trial) Kohn-Sham orbitals obtained by subspace diagonalization. This charge density is then used to evaluate the total energy and calculate an input potential for the next iteration cycle. We note, incidentally, that in the case of an insulator subspace diagonalization becomes unnecessary if $n_\nu(\mathbf{k})$ is equal to the number of occupied bands; the weights w are then equal and

$$\sum_\nu |\phi_{\nu,\mathbf{k}}(\mathbf{r})|^2=\sum_\nu |\Psi_{\nu,\mathbf{k}}(\mathbf{r})|^2$$

by virtue of unitarity. Teter and Allan[19] point out, however, that subspace diagonalization accelerates convergence and therefore is helpful also in calculations for insulators.[26]

Finally, we address briefly the issue of instabilities during self-consistency cycling. We have adopted simple mixing of the output and input charge densities,

$$n_i(t+h)=(1-\gamma)n_i(t)+\gamma n_0(t+h) , \tag{10}$$

where $n_0(t+h)$ is the charge density calculated from the orbitals $\Psi_{\nu,\mathbf{k}}$ updated to time $t+h$, and $n_i(t+h)$ is the charge density from which potentials for the next cycle are determined. In general, the largest feasible mixing coefficient will depend on the time interval h, and the orbital angular momentum of the valence electrons.

C. Pseudopotential

The norm-conserving pseudopotentials proposed by Hamann, Schlüter, and Chiang[27] (HSC) and by Bachelet, Hamann, and Schlüter[28] (BHS) have been widely used. Allan and Teter,[12] however, have noted the convenience of the Kleinman-Bylander[11] fully nonlocal (NL) representation in the context of optimization calculations. Adopting the notation of Ref. 12, we write the matrix elements in the semilocal (SL) representation as

$$\langle \mathbf{q}|V_{\rm SL}|\mathbf{q}'\rangle=\sum_l 4\pi(2l+1)P_l(\cos(\theta_{\mathbf{qq}'}))\times\int dr\, r^2 j_l(qr)j_l(q'r)\delta V_l(r) , \tag{11}$$

and in the KB nonlocal representation as

$$\langle \mathbf{q}|V_{\rm NL}|\mathbf{q}'\rangle=\sum_l 4\pi(2l+1)P_l(\cos(\theta_{\mathbf{qq}'}))\times\int dr\, r^2 j_l(qr)\phi_l(r)\delta V_l(r)\times\frac{\int dr\, r^2 j_l(q'r)\phi_l(r)\delta V_l(r)}{\int dr\, r^2[\phi_l(r)]^2\delta V_l(r)} , \tag{12}$$

where $\phi_l(r)$ is the atomic radial pseudo-wave-function for angular momentum l. The advantage of the nonlocal form is that its operation on a wave function requires $O(M)$ operations, while the semilocal form requires $O(M^2)$, where M is the size of the plane-wave basis set. In the present work we have employed the pseudopotentials $\delta V_l(r)$ compiled by BHS.[27] To generate the corresponding matrix elements of $V_{\rm NL}$, the only additional information required is the atomic radial pseudo-wavefunctions.[29] Most of the numerical calculations described below are based on $V_{\rm NL}$, but for test purposes, a few calculations with $V_{\rm SL}$ were also performed, as discussed in the following section.

$V_{\rm NL}$ and $V_{\rm SL}$ are identical in the case of an isolated atom. Large lattice constant calculations (i.e., in the separated-atom limit) based on $V_{\rm NL}$ should therefore yield eigenfunctions and eigenvalues comparable to those obtained in an atomic calculation based on $V_{\rm SL}$. This correspondence provides a useful self-consistency test on electronic structure codes using the Kleinman-Bylander pseudopotential.[30,31]

III. APPLICATIONS

In this section we present a series of calculations on simple metals with cubic crystal structure, to illustrate the performance of the new methods. Calculations with fixed unit cell volume are described in subsections A–C; in subsection D we discuss calculations in which the unit cell volume as well as the electronic states are optimized simultaneously.

A. Convergence of optimization method

As described above, each iteration of our optimization method consists of a WS update by Eq. (8) followed by a subspace diagonalization. Results of a typical optimization sequence are shown in Fig. 1, based on calculations for bcc Li with the BHS-NL pseudopotential and the fol-

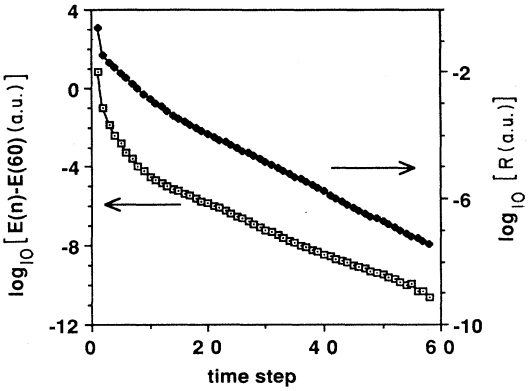

FIG. 1. Optimization sequence for bcc Li with lattice constant $a=5.925$ a.u. Calculations based on $n_k=50$ **k** points, and plane-wave cutoff energy $E_{\rm PW}=24.0$ Ry. The curves show the base-10 logarithm of energy per atom (from which the converged energy [$\approx E(60)$] is subtracted) and the residual R. The linear behavior indicates exponential convergence of both quantities.

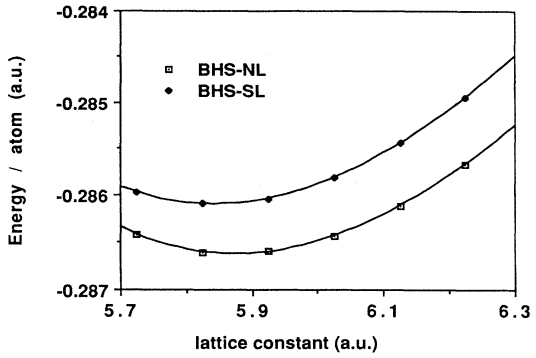

FIG. 2. Binding energy per atom vs lattice constant for bcc Li calculated with the BHS-SL and BHS-NL pseudopotentials. Calculations based on $n_k=12$ and $E_{\rm PW}=18.5$ Ry.

lowing parameters: $n_k=50$ **k** points, $M=485$ plane waves, $n_v(\mathbf{k})=6$ bands, and lattice constant $a=5.925$ a.u. All of the calculations described in this section employed the conventional cubic unit cell, which for the bcc structure includes two atoms. The exchange-correlation potential was represented by the Ceperley-Alder form.[31,32] Initial values of the orbital coefficients $\Psi_i(\mathbf{G}, t=0)$ were assigned using random numbers. We employed the largest time step, $h=2.1$ a.u., for which $E(t_i)$ decreased monotonically. To illustrate energy convergence, Fig. 1 shows the difference between the current value of the energy and its asymptotic value (approximated as the value at iteration 60). The energy curve consists of a short initial transient, during which the initial states are converted into more physical trial wave functions, followed by a linear (note the logarithmic scale) approach to the asymptote. The convergence ratio is roughly 0.75; the energy decreases about 25% of the distance to the asymptote each iteration. Also plotted in Fig. 1 is the rms residual R, defined by the relation

$$R^2=\sum_{\nu,\mathbf{k},\mathbf{G}}|F_{\nu,\mathbf{k}}(\mathbf{G},t)|^2 w(\nu,\mathbf{k})\ . \tag{13}$$

This parameter measures the precision to which the Kohn-Sham equation $F_{\nu,\mathbf{k}}(\mathbf{G})=0$ is satisfied for the occupied states. Both the residual and the energy decrease asymptotically at a comparable rate (note the different ordinate scales).

B. Comparison of SL and NL representations

Computational considerations provide a strong incentive for use of the NL pseudopotential;[12] however, it is important to verify that it yields results comparable to the SL form.[33] In Fig. 2 we show total energies for Li as a function of a calculated with both BHS-SL and BHS-NL pseudopotentials using $n_k=12$ and $M=251$. The results for the two forms differ only in a small, essentially constant energy shift.

C. Lattice constant, bulk modulus, and density of states

Although most previous norm-conserving-pseudopotential calculations for metals have employed variants of the HSC-SL form.[27] we thought it desirable to use the BHS pseudopotentials[28] because of their availability and standardized form. Apparently, simple-cubic phosphorus[34] is the only metal for which results with the BHS pseudopotential have been published. Figure 3 shows total binding energy per atom for this system as a function of lattice constant based on BHS-NL (present work) and BHS-SL (Sasaki *et al.*[34]). The calculations were based on $n_k=60$ and a basis-set cutoff energy of 36 Ry, as in Ref. 34; Sasaki *et al.*, however, used a different zone integration procedure. As we found in Fig. 2, the two curves are similar apart from a nearly constant energy shift. Figure 4 illustrates the electronic density of states for sc P with a lattice constant of 4.63 a.u. A Gaussian-broadening parameter $\sigma=0.02$ was employed. The structure is essentially the same as that given in Ref. 34, but with the Van Hove singularities smeared out by the Gaussian broaden-

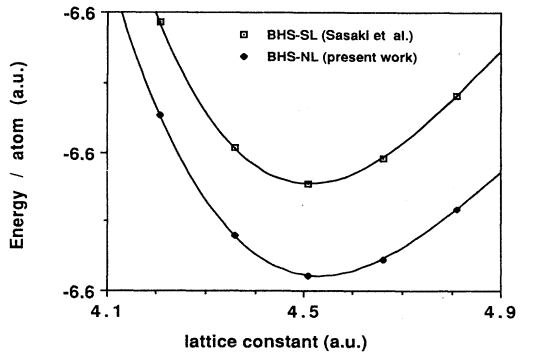

FIG. 3. Binding-energy per atom vs lattice constant for simple-cubic phosphorus calculated with the BHS-NL pseudopotential (present work) and the BHS-SL pseudopotential (Ref. 34). Calculations based on $n_k=60$ and $E_{\rm PW}=36$ Ry.

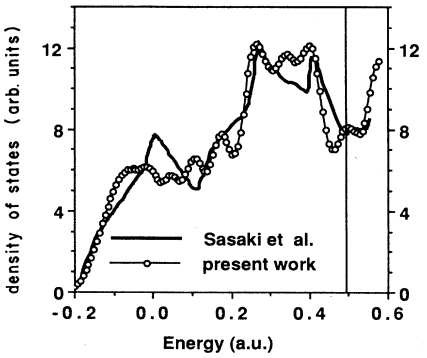

FIG. 4. Density of electronic states for simple-cubic phosphorus taken from Ref. 34 and results of the present work based on the Gaussian-broadening scheme, with $\sigma=0.02$ a.u. Vertical line indicates Fermi level.

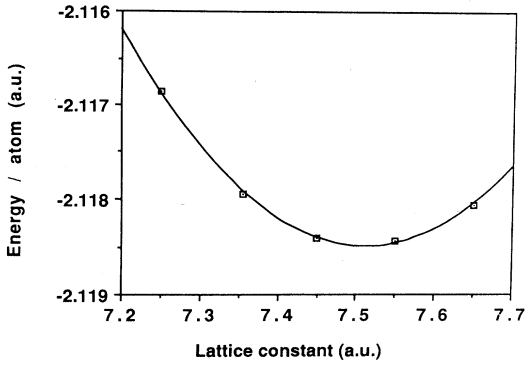

FIG. 5. Binding energy per atom vs lattice constant for fcc Al calculated with the BHS-NL pseudopotential, using $n_k=50$ and $E_{PW}=17$ Ry.

ing. If a more precise density of states were desired, one could use the converged self-consistent potential, calculate a larger number of k points, and apply the tetrahedron method.

The most thoroughly studied metal with norm-conserving pseudopotentials is Al.[35–37] Figure 5 shows results for total binding energy per atom versus lattice constant. The equilibrium lattice constant and bulk modulus calculated from the data in Fig. 5 are listed in Table I, along with results for Li and P. The results for Al are in excellent agreement with previous work as well as with experiment. The results for P are also satisfactory. The predicted lattice constant for Li obtained with BHS-NL are about 10% smaller than experiment. Results for other alkali metals with BHS-NL are similarly poor. Calculations by Dacorogna and Cohen,[38] based on an HSC-SL form with the "partial core correction" procedure of Louie *et al.*,[39] on the other hand, give lattice constants and bulk moduli in much better agreement with experiment; however, the binding energies are somewhat too large. Evidently, property calculations for the alkali metals are sensitive to the pseudopotential.

D. Simultaneous optimization of atomic and electronic degrees of freedom

The simultaneous optimization of both the electronic structure and the atomic configuration, within the local-density approximation, was discussed by Bendt and Zunger.[40] Such a procedure eliminates the need to explicitly map the Born-Oppenheimer surface before optimizing the atomic coordinates. Recent applications[5,12,41] based on dynamical simulated annealing have employed "floating basis sets" to minimize basis set corrections to the Hellmann-Feynman forces, and results have been encouraging.

When a local optimization of the atomic coordinates is sufficient, the steepest-descents methods employed in the present work provide a more direct approach than

TABLE I. Comparison of pseudopotential calculations with experiment. Lattice constant a in a.u., bulk modulus B in Mbar, and binding energy per atom E_0 in hartrees. Results not corrected for zero-point motion. BHS-NL and BHS-SL calculations for Li based on $n_k=12$, cutoff energy $E_{PW}=18.5$ Ry; BHS-NL calculations with $n_k=50$, $E_{PW}=24$ Ry yielded $a=5.97$ a.u., $B=0.1634$, and $E_0=0.277$ Ry. BHS-NL calculations for (Al,K,P) employed $n_k=(50,12,60)$ and $E_{PW}=(17.0,6.0,36)$ Ry.

	Property	BHS-NL	BHS-SL	HSC-SL	Expt.
bcc Li	a	5.88	5.84	6.43[a]	6.59
	B	0.174	0.177	0.130	0.131
	E_0	0.2874	0.2866	0.310	0.259
fcc Al	a	7.51		7.58[b]	7.60
	B	0.715		0.715	0.722
	E_0	2.118		2.096	2.081
sc P	a	4.55	4.52[c]	4.72[d]	4.68
	B	1.18	1.27	0.956	0.950
	E_0	6.64	6.63	6.57	

[a]Reference 38.
[b]Reference 35.
[c]Reference 34.
[d]Reference 44.

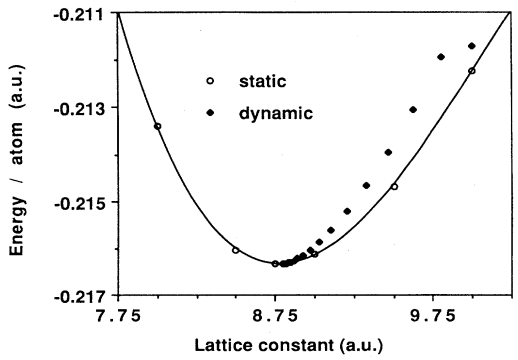

FIG. 6. Binding energy per atom vs lattice constant for bcc K, with $n_k=12$ and $E_{\rm PW}=6$ Ry. Values labeled "static" correspond to separate optimizations at fixed lattice constant. Values labeled "dynamic" represent the results of simultaneous optimization of electronic structure and lattice constant.

dynamical simulated annealing. In the work described in this section, we have simultaneously optimized the electronic structure and the atomic volume; these methods can also be adapted to treat less symmetric relaxations, such as the strain surrounding an impurity.

In the present treatment, the electronic structure is calculated using the Williams-Soler algorithm, Eq. (8), while the atomic volume is adjusted each time step by the steepest-descent prescription

$$\Omega(t+h)=\Omega(t)+ph/\nu_\Omega\ , \tag{14}$$

where p is the present and ν_Ω is the effective "viscosity." The calculation of the pressure is outlined in Appendix B. The viscosity is an arbitrary parameter whose value must be chosen small enough to enable the atomic volume to adjust itself to relieve the pressure, but large enough to avoid the numerical instabilities that would result from rapid volume fluctuations. The results of such a calculation for bcc K, labeled "dynamic," along with converged results for fixed lattice constant, labeled "static," are plotted in Figs. 6 and 7. The electronic states for the dynamic run were "initialized" by iterating Eq. (8) for 10 time intervals $h=1.6$ a.u. (starting from random states, as described in Sec. II) with a fixed lattice constant $a=10$ a.u. Subsequently, Eqs. (8) and (14) were employed to update the electronic states and the atomic volume simultaneously, using a viscosity $\nu_\Omega=10^{-6}$ a.u. The results for the energy and the pressure are plotted in Figs. 6 and 7, respectively. The lattice constant and the pressure exhibit exponential behavior, with no overshoot. The present procedure has enabled us to determine the equilibrium lattice constant as well as the self-consistent electronic structure in the same number of iterations as normally employed to achieve convergence in static-lattice calculations.

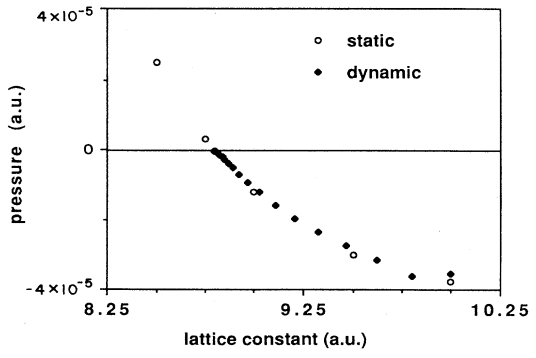

FIG. 7. Pressure vs lattice constant for bcc K. See caption to Fig. 6.

IV. DISCUSSION

The key elements of the optimization method developed in this paper are (i) the Williams-Soler algorithm, (ii) subspace diagonalization, (iii) the plane-wave basis set, and (iv) the fully nonlocal pseudopotential of the Bylander-Kleinman form. The convergence of the method was excellent in applications to simple metals. Our comparisons of the BHS-NL with the BHS-SL pseudopotentials were also encouraging and suggest that the two forms will normally give comparable results. Furthermore, although the pathological behavior mentioned in Ref. 33 may occur in some instances, it can be remedied straightforwardly.

The agreement of calculated properties with experiment, as usual, depends on the quality of the pseudopotential. Although the concept of norm conservation has put first-principles pseudopotentials on a much sounder basis, it does not, of course, guarantee correct physical behavior. The results on the alkalis are a case in point. More work on the development of reliable pseudopotentials for condensed matter applications therefore seems warranted.

With the testing of our methods on elemental metals completed, treatment of more complex atomic arrangements such as intermetallic compounds and disordered systems is now possible. Work along these lines is now in progress.

ACKNOWLEDGMENTS

This work was supported by the U.S. Department of Energy (Division of Materials Sciences of the Office of Basic Energy Sciences), under Contract No. W-31-109-ENG-38. Computational work was performed at the National Magnetic Fusion Energy (NMFE) Computing Center at Lawrence Livermore National Laboratory, on the Cyber 205 computer at ETA Systems, St. Paul, Minnesota, and at the Florida State University (FSU) Supercomputer Computations Research Institute, which is partially funded by the U.S. Department of Energy under Contract No. DE-FC05-85ER25000. B. I. Min was supported in part by the Pohang Institute of Technology. J. Garner was supported financially by Bradley University and the Division of Educational Programs at Argonne National Laboratory. The authors gratefully acknowledge discussions with R. K. Kalia and D. D. Koelling.

APPENDIX A: GAUSSIAN-BROADENING METHOD

This appendix outlines the formulation of the Gaussian-broadening method, which is employed in Brillouin-zone integrations. The density of states in this method is expressed as

$$N(\epsilon)=\sum_{\nu,\mathbf{k}} g(\epsilon-\epsilon_{\nu\mathbf{k}})\Omega(\mathbf{k}) , \tag{A1}$$

where the "line-shape function" is represented by a Gaussian $g(x)=[(2\pi)^{1/2}\sigma]^{-1}\exp(-x^2/2\sigma^2)$ whose width σ is commensurate with the energy-level spacing. By integrating the line-shape function up to the Fermi energy, we obtain the occupancy factor

$$z(\epsilon_F-\epsilon_{\nu\mathbf{k}})=\{1+\mathrm{erf}[(\epsilon_F-\epsilon_{\nu\mathbf{k}})/\sqrt{2}\sigma]\}/2 . \tag{A2}$$

In calculating properties such as total energy, one requires integrals of some energy-dependent function $y(\epsilon)$ weighted by the density of states,

$$I[y]=\int_{-\infty}^{\epsilon_F} y(\epsilon)N(\epsilon)d\epsilon . \tag{A3}$$

Substituting Eq. (A1) into Eq. (A3), and expanding y to first order about $\epsilon_{\nu\mathbf{k}}$, we obtain

$$I[y]=\sum_{\nu,\mathbf{k}} \Omega(\mathbf{k})[y(\epsilon_{\nu,\mathbf{k}})z(\epsilon_F-\epsilon_{\nu\mathbf{k}}) -\sigma^2 y'(\epsilon_{\nu,\mathbf{k}})g(\epsilon_F-\epsilon_{\nu\mathbf{k}})] . \tag{A4}$$

Two cases of importance are the sum of eigenvalues ($y=\epsilon$, $y'=1$) for occupied states and the charge density ($y=|\phi(r)|^2$). In the former case we have

$$I[\epsilon]=\sum_{\nu,\mathbf{k}} w(\nu,\mathbf{k})\epsilon_{\nu,\mathbf{k}}-\sigma^2 N(\epsilon_F) . \tag{A5}$$

The first term in Eq. (A5) is the weighted sum of the discrete eigenvalues and the second term is a correction for the levels whose line-shape function g overlaps with ϵ_F. The correction term is typically small, but has been included in the numerical calculations described in Sec. III. In the case of the charge density ($y=|\phi(r)|^2$), however, Eq. (9) has been employed without a correction term proportional to σ^2; such a term would average to zero over the unit cell because of wave-function normalization.

APPENDIX B: CALCULATION OF TOTAL ENERGY AND PRESSURE

Ihm *et al.*[42] developed a momentum-space formulation of the total energy of a solid for use in conjunction with first-principles pseudopotentials. The energy calculations in the present paper were based on the framework established in that work, adapted to the Gaussian-broadening integration scheme (Appendix A). In the local-density approximation, the total energy of a solid per atom is written as the sum of (single-particle) kinetic energy E_K, Coulomb energy $(=E_{ee}+E_{ii}+E_{ie})$, and exchange-correlation energy E_{xc}, which can be expressed in the form[42]

$$E=\int_{-\infty}^{\epsilon_F} N(\epsilon)\epsilon\, d\epsilon+\int[\epsilon_{\mathrm{xc}}(n(\mathbf{r}))-\mu_{\mathrm{xc}}(n(\mathbf{r}))]n(\mathbf{r})d^3r -\tfrac{1}{2}\sum_{\mathbf{G}\,(\neq 0)} V_{ee}(\mathbf{G})n(\mathbf{G})+\alpha_1 Z_v+\gamma_{\mathrm{Ewald}} , \tag{B1}$$

where the first term represents the sum of the single particle eigenvalues, the second term corrects for exchange and correlation, the third term corrects for double counting, and the last two terms account for the Ewald energy, corrected for the $(\mathbf{G}=\mathbf{0})$ component of the local part of the pseudopotential. The eigenvalue sum is evaluated using Eq. (A5). The second and third terms are determined by the charge density $n(\mathbf{r})$, which is calculated with Eq. (9). The last two terms do not depend on the eigenstates; they depend only on the atomic configuration, the volume, and the pseudopotentials. An expression for the pressure can be obtained by differentiating Eq. (B1) with respect to volume (see, e.g., Nielsen and Martin[43]):

$$p=-\partial E/\partial\Omega =p_K+p_{\alpha 1}+p_{ei,L}+p_{ei,\mathrm{NL}}+p_{ee}+p_{\mathrm{Ewald}}+p_{\mathrm{xc}} . \tag{B2}$$

The contribution from kinetic energy is given by $p_K=2E_K/3\Omega$. The mean value of the pseudopotential gives rise to a pressure $p_{\alpha 1}=\alpha_1 Z_V/\Omega$. The local part of the electron-ion contribution $p_{ei,L}$ is given by the derivative of

$$E_{ei,L}\equiv\sum_{\mathbf{G}\,(\neq 0)} V_{ei,L}(\mathbf{G})n(\mathbf{G}) .$$

Here the local part of the BHS pseudopotential (for each species in a multicomponent system) is written

$$V_{ei,L}(\mathbf{G})=-4\pi Z_V S(\mathbf{G})/(G^2\Omega)\sum_{i=1}^{2} c_i\exp(-G^2/4\alpha_i) ,$$

where Z_V is the number of valence electrons in the unit cell with volume Ω, $S(\mathbf{G})\equiv\sum_\mu\exp(-i\mathbf{G}\cdot\mathbf{R}_\mu)$ is the unit-cell structure factor, and the numerical constants c_i and α_i [not to be confused with α_1 in Eq. (B1)] are tabulated in Ref. 28. The explicit result is

$$p_{ei,L}=-E_{ei,L}/(3\Omega)-4\pi Z_v/(6\Omega^2) \times\sum_{\mathbf{G}\,(\neq 0)} S(\mathbf{G})n(\mathbf{G}) \times\sum_i (c_i/\alpha_i)\exp(-G^2/4\alpha_i) .$$

The nonlocal part of the electron-ion interaction energy can be written as

$$E_{ei,\mathrm{NL}}=4\pi\Omega^{-1}\sum_{i,\mu}\sum_{\mathbf{G},\mathbf{G}'}\Psi_i^*(\mathbf{k}+\mathbf{G}')\Psi_i(\mathbf{k}+\mathbf{G}) \times\exp[i(\mathbf{G}-\mathbf{G}')\cdot\mathbf{R}_\mu] \times\langle\mathbf{q}'|V_{\mathrm{NL}}|\mathbf{q}\rangle ,$$

where $\mathbf{q}\equiv\mathbf{k}+\mathbf{G}$, $\mathbf{q}'\equiv\mathbf{k}+\mathbf{G}'$, and the matrix element of the separable-kernel form of V_{NL} can be factored as[12]

$$\langle\mathbf{q}'|V_{\mathrm{NL}}|\mathbf{q}\rangle=\sum_\Lambda v_\Lambda^*(\mathbf{q}')v_\Lambda(\mathbf{q}) \tag{B3}$$

in terms of the vectors

$$v_\Lambda(\mathbf{q}) \equiv (4\pi)^{1/2} Y_\Lambda(\mathbf{q}) \int dr\, r^2 j_l(qr) \Delta V_l(r) ,$$

with the collective angular momentum index $\Lambda \equiv \{l,m\}$ and

$$\Delta V_l(r) \equiv \phi_l(r) \delta V_l(r) \left[\int dx\, x^2 [\phi_l(x)]^2 \delta V_l(x) \right]^{-1/2} ;$$

here $\phi_l(r)$ is the atomic pseudo-wave-function and $\delta V_l(r)$ is the nonlocal pseudopotential component for angular momentum l. Differentiating $E_{ei,NL}$, we obtain

$$p_{ei,\mathrm{NL}} = E_{ei,\mathrm{NL}}/\Omega + (3\Omega^2)^{-1} \sum_{\Lambda,\mu} \sum_{\mathbf{G},\mathbf{G}'} \Psi_i^*(\mathbf{k}+\mathbf{G}') \Psi_i(\mathbf{k}+\mathbf{G}) \exp[i(\mathbf{G}-\mathbf{G}')\cdot\mathbf{R}_\mu] \left[\frac{\partial v_\Lambda(q)}{\partial \ln q} v_\Lambda(q') + \frac{\partial v_\Lambda(q')}{\partial \ln q'} v_\Lambda(q) \right] .$$

The potential components $v_\Lambda(q)$ and the derivatives $\partial v_\Lambda(q)/\partial \ln q$ may be calculated once and for all and stored in tabular form for each atomic species.

The remaining terms in Eq. (B2) are obtained straightforwardly: $p_{ee} = E_{ee}/3\Omega$, $p_{\mathrm{Ewald}} = E_{\mathrm{Ewald}}/3\Omega$, and $p_{\mathrm{xc}} = (\mu_{\mathrm{xc}} - E_{\mathrm{xc}})/\Omega$.

*Permanent address: Department of Physics, Michigan Technological University, Houghton, MI 49931.

†Permanent address: Department of Physics, Pohang Institute of Science and Technology, Pohang 680, Seoul, Korea.

‡Permanent address: Department of Physics, Bradley University, Peoria, IL 61625.

[1]O. K. Andersen and O. Jepsen, Phys. Rev. Lett. **53**, 2571 (1985).

[2]J. Hafner, J. Phys. F **18**, 153 (1988); S. S. Jaswal and J. Hafner, Phys. Rev. B **38**, 7311 (1988); J. Hafner and S. S. Jaswal, *ibid.* **38**, 7320 (1988).

[3]S. K. Bose, K. Winer, and O. K. Andersen, Phys. Rev. B **37**, 6262 (1988); S. K. Bose, S. S. Jaswal, O. K. Andersen, and J. Hafner, *ibid.* **37**, 9955 (1988).

[4]See, e.g., D. M. Wood and A. Zunger, J. Phys. A **18**, 1343 (1985); J. L. Martins and M. L. Cohen, Phys. Rev. B **37**, 6134 (1988); C. M. M. Nex, J. Comp. Phys. **70**, 138 (1987).

[5]R. Car and M. Parrinello, Phys. Rev. Lett. **55**, 2471 (1985); **60**, 204 (1988).

[6]R. Car, M. Parrinello, and W. Andreoni, in *Proceedings of the First NEC Symposium on Fundamental Approaches to New Material Phases,* edited by S. Sugano, Y. Nishina and S. Ohnishi (Springer, Berlin, 1987), p. 134; D. Hohl, R. O. Jones, R. Car, and M. Parrinello, Chem. Phys. Lett. **139**, 540 (1987); J. Chem. Phys. (to be published); R. Car and M. Parrinello, in *The Physics of Semiconductors,* edited by O. Engström (World Scientific, Singapore, 1986), p. 1165; P. Ballone, W. Andreoni, R. Car, and M. Parrinello, Phys. Rev. Lett. **60**, 271 (1988); G. Galli, R. M. Martin, R. Car, and M. Parrinello (unpublished).

[7]A. R. Williams and J. Soler, Bull. Am. Phys. Soc. **32**, 562 (1987).

[8]M. C. Payne, J. D. Joannopoulos, D. C. Allan, M. P. Teter, and D. H. Vanderbilt, Phys. Rev. Lett. **56**, 2656 (1986).

[9]J. Garner, S. G. Das, B. I. Min, C. Woodward, and R. Benedek (unpublished).

[10]Williams and Soler employed an augmented-plane-wave (APW) basis in their work (Ref. 7).

[11]L. Kleinman and D. M. Bylander, Phys. Rev. Lett. **48**, 1425 (1982).

[12]D. C. Allan and M. Teter, Phys. Rev. Lett. **59**, 1136 (1987).

[13]C. L. Fu and K.-M. Ho, Phys. Rev. B **28**, 5480 (1983).

[14]M. H. Kang, R. C. Tatar, E. J. Mele, and P. Soven, Phys. Rev. B **35**, 5457 (1987).

[15]M. C. Payne, P. D. Bristowe, and J. D. Joannopoulos, Phys. Rev. Lett. **58**, 1348 (1987); M. Needels, M. C. Payne, and J. D. Joannopoulos, *ibid.* **58**, 1765 (1987).

[16]K. E. Schmidt and M. H. Kalos, in *Applications of the Monte Carlo Method in Statistical Physics,* edited by K. Binder (Springer, New York, 1984), p. 145.

[17]This minimum will normally correspond to the ground state. Metastable states cannot be ruled out *a priori*, but experience indicates that they are rare in the context of the local-density approximation (LDA). In the limiting case of noninteracting electrons in an external potential, excited states can be shown to correspond to saddle points (Ref. 9), and metastable states therefore do not occur.

[18]It is understood that $H_{\mathbf{G}\mathbf{G}'}$ also depends on the wave vector $\mathbf{k}$.

[19]M. Teter and D. C. Allan, unpublished, treat the time dependence of $\beta_i(\mathbf{G},t)$ phenomenologically. They obtain a relation identical to Eq. (8), with a modified argument in the function $f(x)$.

[20]M. C. Payne, M. Needels, and J. D. Joannopoulos, Phys. Rev. B **37**, 8138 (1988).

[21]P. R. Adby and M. A. H. Dempster, *Introduction to Optimization Methods* (Wiley, New York, 1974), p. 57.

[22]The time interval h was held constant in our treatment. Alternatively, one could optimize h between successive force calculations; however, total-energy calculations are not significantly less time consuming than force calculations.

[23]R. Benedek, B. I. Min, C. Woodward, and J. Garner, in *Computer Simulation Studies in Condensed Matter Physics: Recent Developments,* edited by D. P. Landau and H.-B. Schüttler (Springer, Berlin, 1989).

[24]H. J. F. Jansen and A. J. Freeman, Phys. Rev. B **30**, 561 (1984).

[25]We are indebted to H. J. F. Jansen for the use of his computer code for generating $\mathbf{k}$-point sets. The first points selected are high-symmetry points at the zone center and at zone boundaries; for the simple-cubic supercells employed in the present work there are four such points: Γ, M, X, and R.

[26]In the limit of large $n_v(k)$ and small time step h, our approach becomes equivalent to standard diagonalization methods. In this context, the optimization procedure based on Eq. (8) may be viewed as an elaborate basis-set contraction method.

[27]D. R. Hamann, M. Schlüter, and C. Chiang, Phys. Rev. Lett. **43**, 1494 (1979).

[28]G. B. Bachelet, D. R. Hamann, and M. Schlüter, Phys. Rev. B **26**, 4199 (1982).

[29]We are grateful to D. D. Koelling for an updated version of the Liberman-Waber-Cromer code, which was used to calculate atomic pseudo-wave-functions.
[30]D. C. Allan (private communication).
[31]D. M. Ceperley and B. J. Alder, Phys. Rev. Lett. **45**, 566 (1980).
[32]J. Perdew and A. Zunger, Phys. Rev. B **23**, 5048 (1981).
[33]A pitfall was noted in footnote 10 of Ref. 11: the breakdown of core exclusion. This did indeed occur for the BHS-NL pseudopotential in the case of K. The problem may be remedied by a reapportionment of the total potential between the local and the l projected parts.
[34]T. Sasaki, K. Shindo, K. Niizeki, and A. Morita, Solid State Commun. **62**, 795 (1987).
[35]P. K. Lam and M. L. Cohen, Phys. Rev. B **24**, 4224 (1981).
[36]B. Chakraborty and R. W. Siegel, Phys. Rev. B **27**, 4535 (1983).
[37]C. O. Rodriguez, O. M. Cappannini, E. L. Peltzer y Blanca and R. A. Casali, Phys. Status Solidi B **412**, 353 (1987).
[38]M. M. Dacorogna and M. L. Cohen, Phys. Rev. B **34**, 4996 (1986).
[39]S. G. Louie, S. Froyen, and M. L. Cohen, Phys. Rev. B **26**, 1738 (1982).
[40]P. Bendt and A. Zunger, Phys. Rev. Lett. **50**, 1684 (1983).
[41]M. R. Pederson, B. M. Klein, and J. Q. Broughton, Phys. Rev. B **38**, 3825 (1988).
[42]J. Ihm, A. Zunger, and M. L. Cohen, J. Phys. C **12**, 4409 (1979).
[43]O. H. Nielsen and R. M. Martin, Phys. Rev. B **32**, 3780 (1985); **32**, 3792 (1985).
[44]K. J. Chang and M. L. Cohen, Phys. Rev. B **33**, 6177 (1986).